Hindawi
Geofluids
Volume 2021, Article ID 9508367, 13 pages
https://doi.org/10.1155/2021/9508367

Research Article

Loading Behavior and Soil-Structure Interaction for a Floating Stone Column under Rigid Foundation: A DEM Study

Feng Liu,[1] **Panpan Guo**,[1] **Haibo Hu**,[1] **Chengwei Zhu**,[1,2] **and Xiaonan Gong**[1]

[1]*Research Center of Coastal and Urban Geotechnical Engineering, Zhejiang University, Hangzhou 310058, China*
[2]*Institute of Geotechnical Engineering, University of Natural Resources and Life Sciences Vienna, Vienna 1180, Austria*

Correspondence should be addressed to Panpan Guo; pp_guo@zju.edu.cn and Chengwei Zhu; zhuchengwei@zju.edu.cn

Received 12 August 2021; Accepted 30 August 2021; Published 21 September 2021

Academic Editor: Yu Wang

This paper investigates the loading behavior and soil-structure interaction associated with a floating stone column under rigid foundation by using the discrete element method (DEM). The aggregates and soft soil are simulated by particles with different sizes. The rigid foundation is simulated by two loading plates at the same position with the same velocity. The stress distributions and microscopic interaction between the column and soft soil are investigated. The vertical stress of the column increases with settlement and decreases with the depth. The position of the column with large radial stress also has large deformation, which decreases from top to bottom. The vertical and radial stresses of the soft soil increase with settlement, and the radial stress shows high value in the upper part of soft soil. The stress concentration ratio is obtained by two loading plates, which decreases from 2.5 to 1.55 during loading. The interaction between column and soft soil shows that the column does not penetrate into the underlying stratum but drags the surrounding soil down.

1. Introduction

Stone columns have been proved to be effective, economical, and environment friendly to improve the soft soils [1, 2]. They can increase bearing capacity, reduce final and differential settlement, accelerate soil consolidation, improve slope stability, and decrease liquefaction potential [3–5]. Since this technique was first recorded in 1839 in Bayonne (France), it has been widely used around the world [6–8]. Numerous studies have been done to reveal the engineering characteristics of stone column-improved soft soils, especially in recent decades.

Based on one-dimensional (1D) consolidation theory by Terzaghi and ideal drain well solution by Barron, many analytical, semianalytical solutions of soft clay with stone column have been obtained. Most of them considered pore water pressure and time factor, derived consolidation equations under various geological states and boundary conditions. The average degree of consolidation can be well predicted by using the solutions [9–15].

Field monitoring can get the settlement and deformation of structure; the data can be used to reliably analyze settlement and bearing capacity of stone columns in soft clay. In situ monitoring generally lasts for several years, even more than ten years, which is time-consuming and uneconomical [1, 2]. Laboratory tests can overcome those disadvantages, which simulate field structure in small scale. Experimental study on behavior of stone column can be carried out by various parameters like shear strength of soft clay, loading conditions, and diameter and spacing of stone columns [16–21]. Obvious bulging deformation can be observed when only pile is loaded; the maximum bulging location is 0.5 times the column diameter from the top [20]. No significant bulging is seen when the load is applied to the entire model tank area [20, 21].

The finite element method (FEM) is widely used to analyze the behavior of stone columns. It is assumed that stone column is isotropic and continuous, and part of the model is usually taken as research object due to the axial symmetry [22–30]. Some studies convert individual stone columns to

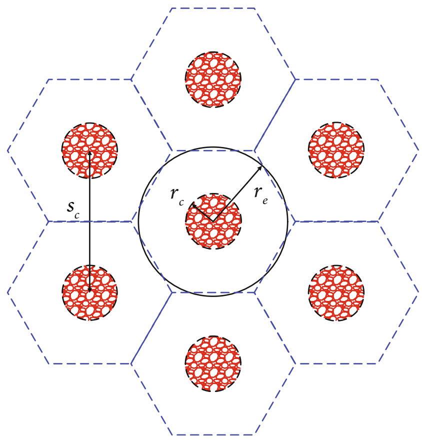

(a) Triangular

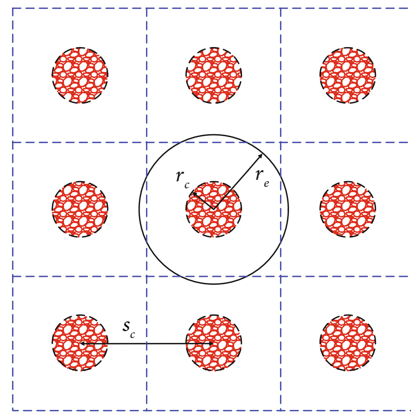

(b) Square

Figure 1: Layout of stone columns.

column walls using plane strain analysis. The results coincide with equivalent area method in long-term conditions [26]. The computational efficiency of FEM is relatively high, but its results mainly focus on the macroscopic level of model.

DEM-FDM is a coupled numerical modeling scheme. Isolated stone column can be simulated by DEM, and surrounding soil is simulated by FDM with Mohr-Coulomb yield criterion. Many studies using this method have been done to understand the behavior of stone columns and surrounding soils [31–35]. It is found that the failure mode of isolated stone column in soft clay is related to soil elastic modulus and soil cohesion [31]. The force and displacement between stone column and soil are transferred by a series of walls, which cannot be captured directly.

The DEM is widely used in geotechnical engineering, such as slopes, embankments, roads, and rocks [36–46]. In geotechnical engineering, DEM can simulate the discontinuity of soil and rock and reveal the microscopic failure mechanism. Wang et al. [40] have used DEM to study the effects of confining pressure and load path on deformation and strength of cohesive granular materials. Yu et al. [42] have investigated the failure mechanism of sandstones under different bedding angles and osmotic pressures by DEM. DEM is an effective simulation method because of the granularity of stone column aggregate; it can simulate microscopic response of granular materials. Gu et al. built a 3D DEM model for an end-bearing stone column in soft clay, and the stone column and surrounding soil were simulated by DEM. They analyzed the stress and deformation of an isolated stone column under load [47]. However, in practice, stone columns do not always penetrate the soft soil layer and sit on a hard bearing layer [19, 21]. Stone columns are ordinary installed under rigid foundation or uniform distributed load [22]. Until now, according to the author's knowledge, there is no DEM research on the stress and deformation of floating stone column under rigid foundation.

In this study, a 3D model for floating stone column in soft clay is built, and the model is loaded uniformly on the top. The vertical and radial stress of the column and the soft soil, the porosity, coordination number and deformation of the column, the stress concentration ratio, and the column-soil interaction are analyzed.

Table 1: Microscopic properties of aggregate.

Parameter	Value
Particle density (g/cm^3)	2.65
Coefficient of particle friction	0.8
Particle normal stiffness (N/m)	6.0×10^7
Particle shear stiffness (N/m)	1.0×10^7
Contact bond normal strength (N)	130
Contact bond shear strength (N)	130

Table 2: Microscopic properties of soil particles in the top layer.

Parameter	Value
Particle density (g/cm^3)	2.65
Coefficient of particle friction	0.25
Particle normal stiffness (N/m)	4.0×10^4
Particle shear stiffness (N/m)	4.0×10^4
Contact bond normal strength (N)	3.2
Contact bond shear strength (N)	3.2

2. Numerical Simulation

2.1. Unit Cell. Stone columns are usually arrayed in triangular or square as depicted in Figure 1. Thus, the part of column and surrounding soil is a hexagon (Figure 1(a)) or square (Figure 1(b)). Due to axial symmetry conditions, the hexagon or square can be transformed into a circle (cylinder) with the same area. The diameter of unit cell is $2r_e = 1.05 - 1.13s_c$ for triangular and square form, respectively, where s_c is the distance from center to center between

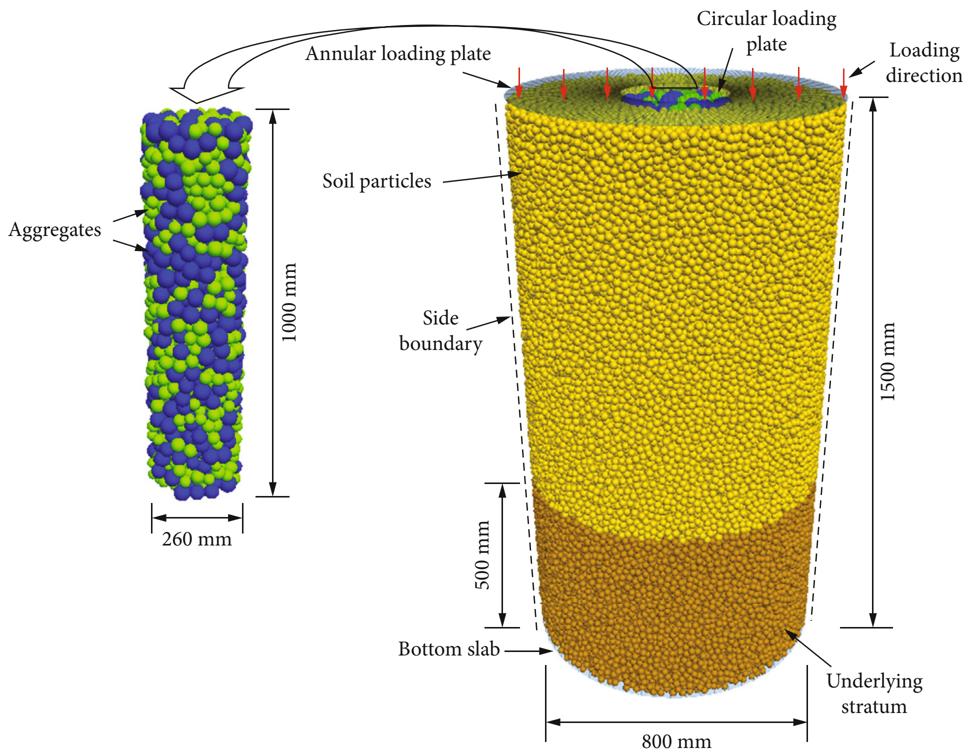

FIGURE 2: 3D model for unit cell of a floating stone column in soft clay.

columns, r_c is the radius of the column, and r_e is the replacement radius of the column.

2.2. Parameter Selection. The DEM software, three-dimensional particle flow code (PFC3D, version 5.0), is applied in this study. PFC is a mature business software of Itasca company. The displacements and contact forces of each particle are calculated by Newton's second law.

The linear contact bond model is used in this study to simulate the aggregate and the soft clay. The parameters of aggregates and soil particles are shown in Tables 1 and 2, which have been validated by Gu. In the Gibson soil model, the undrained shear strength of soft clay increases with depth. According to Han's suggestion, the undrained shear strength of soft clay can be calculated [48]:

$$\tau_u = c + 0.25\gamma' z, \tag{1}$$

where c is the cohesion of soft clay and γ' is the effective specific weight of soft clay. The contact-bond strength of the lower six layers was 3.40 N, 3.65 N, 3.95 N, 4.20 N, 4.55 N, and 4.90 N, respectively.

2.3. DEM Model of a Floating Stone Column under Rigid Foundation. A 3D DEM model is built to simulate a floating stone column under rigid foundation. Figure 2 shows the unit cell for a floating stone column in soft clay. In order to effectively simulate stone column-soil interaction and improve the calculation efficiency, the diameter and height of the model are set as 800 mm and 1500 mm, respectively.

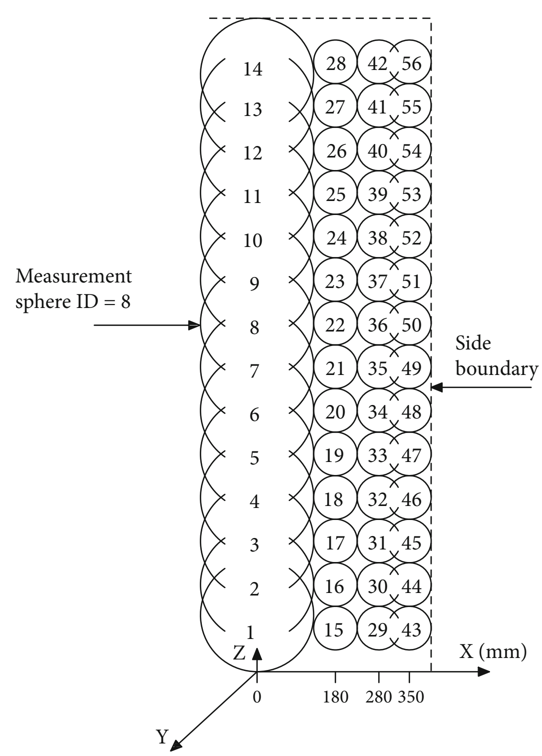

FIGURE 3: Position of measurement spheres within the model.

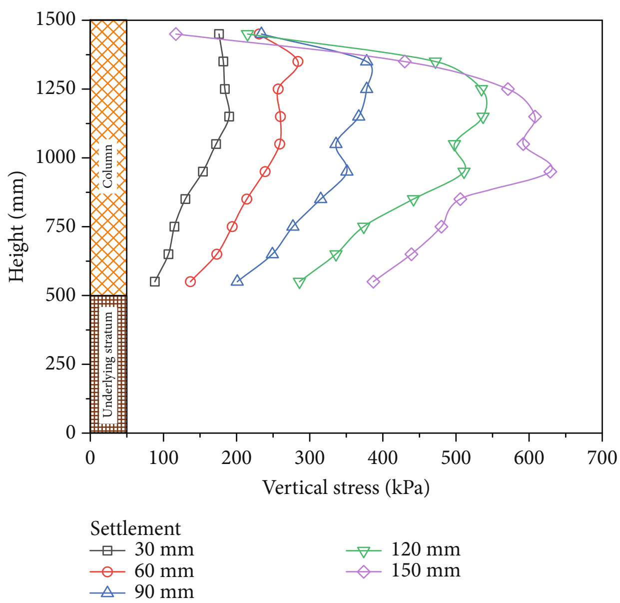

Figure 4: Vertical stresses of stone column under different settlements.

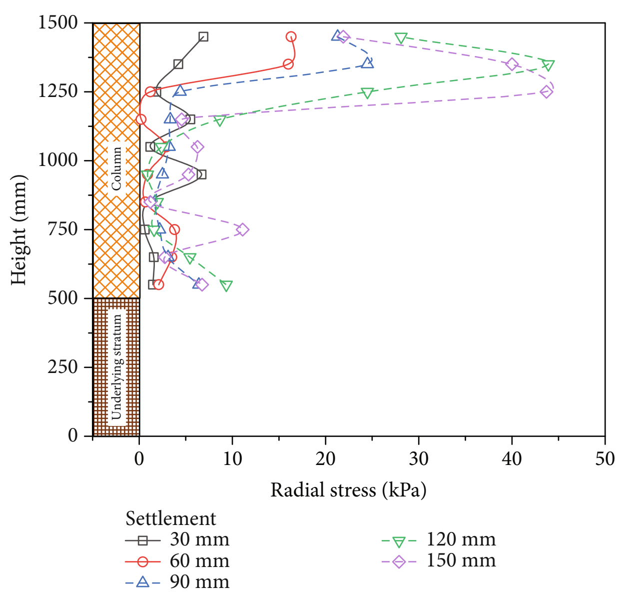

Figure 5: Radial stresses of stone column under different settlements.

The bottom slab of the model is fixed. The friction coefficient of side boundary is set as 0 to reduce the influence of the boundary on the model. The diameter of stone column is 260 mm, and the length is 1000 mm. The diameter of aggregates ranges from 30 to 50. Aggregates with a diameter of 30 to 40 mm make up 40% of the stone column, and aggregates with a diameter of 40-50 mm make up 60%. The porosity of stone column is 0.37. The area replacement ratio is 10.56%, between 10 and 35% [7].

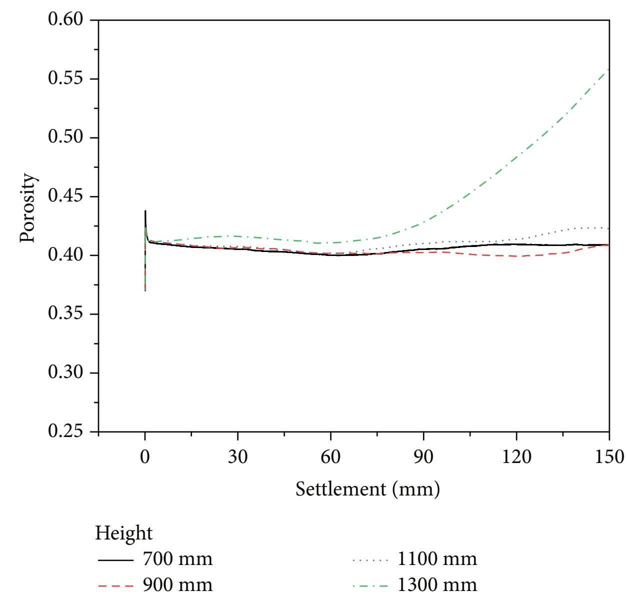

Figure 6: Porosity changes of the column during loading.

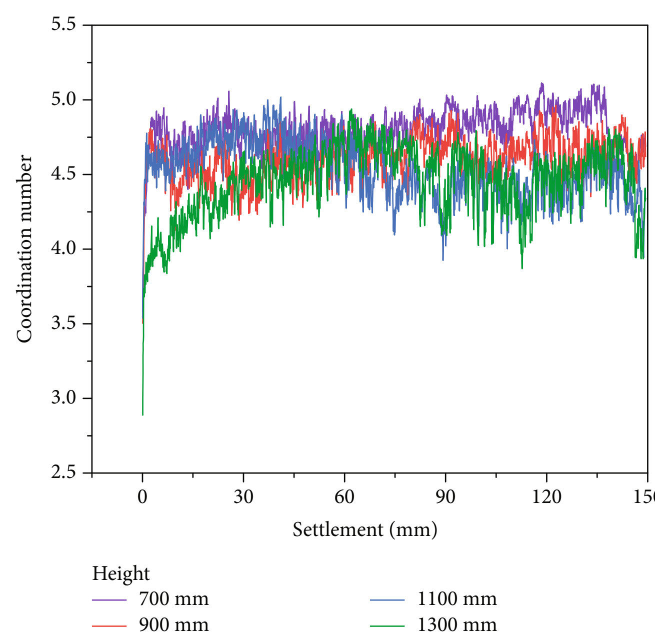

Figure 7: Coordination number in the column during loading.

Due to the irregular shape of soil particles and the influence of mineral component, the microscopic interaction of soil particles is very complex [49, 50]. DEM is difficult to simulate clayey soil accurately. This study makes some simplifications, ignores some properties, and focuses on the cohesive features of soft clay. The soft clay is simulated by linear contact bond model. The diameter of soil particles ranges from 18 to 20 mm. A total of 117930 particles are generated to simulate soft clay around and beneath the stone column. For clear display, the soil particles are divided into two groups, the soil around stone column and the

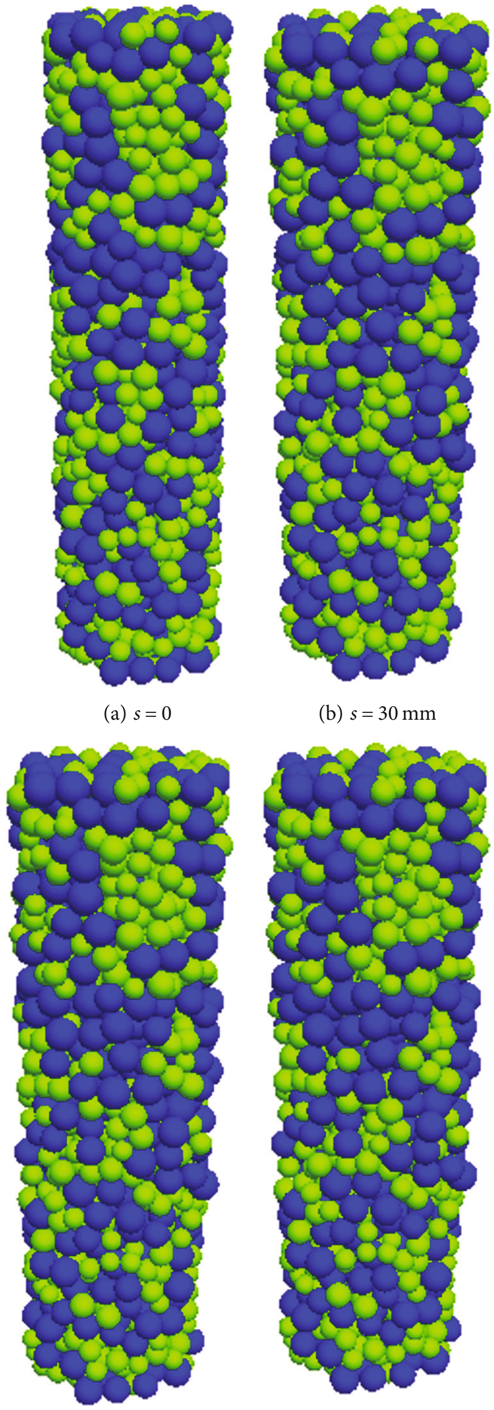

(a) $s = 0$ (b) $s = 30$ mm

(c) $s = 60$ mm (d) $s = 90$ mm

Figure 8: Continued.

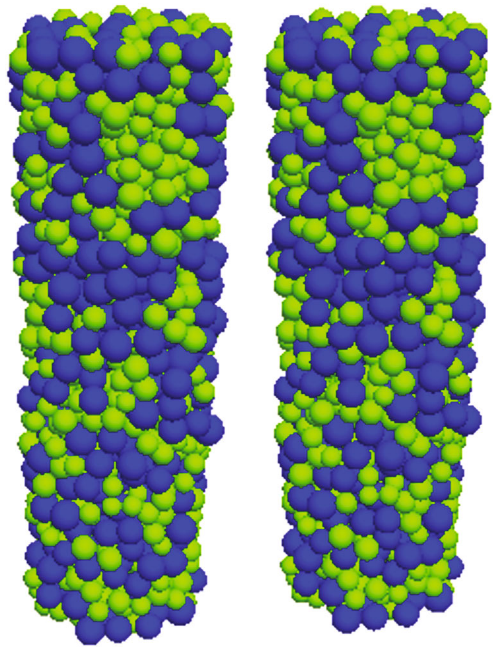

(e) $s = 120\,\text{mm}$ (f) $s = 150\,\text{mm}$

Figure 8: Deformation of the column during loading.

underlying stratum, which are shown in different colors. The initial porosity of soft clay is 0.4.

A circular plate and an annular plate are generated as loading plates. The two loading plates are rigid and will not be deformed during the loading process. The diameter of the circular plate is 260 mm. The inner diameter of the annular is 260 mm and the outer diameter is 800 mm. The two loading plates move down simultaneously to obtain an initial pressure of 5.0 kPa. Under the initial pressure, the particles of stone column and soil reach a certain compaction state. The displacement control method is used in the loading process. During the loading process, the two loading plates simultaneously move downward at a uniform speed of 0.008 m/s. This speed is small enough to ensure that the model remains quasistatic during loading. The ratio of the maximum unbalanced force to the maximum contact force is less than 0.003.

The parameter variation of aggregates and soft clay during loading can be monitored by measurement spheres. Figure 3 shows the location of measurement spheres within the model. There are fourteen measurement spheres of 260 mm diameter along the stone column to the bottom slab. These measurement spheres (ID from 1 to 14) overlapped each other, allowing for more intensive monitoring of data. Forty-two measurement spheres (ID from 15 to 56) are generated to monitor the surrounding soft soil at different position. The diameter of these measurement spheres is 100 mm.

3. Results

3.1. Stresses and Deformation of the Stone Column. The measurement sphere provided by PFC3D 5.0 can effectively obtain the stress and deformation changes of the column and soil clay during loading. Because the medium is discrete, stress cannot be obtained directly. The average stress in a measurement sphere can be computed:

$$\bar{\sigma} = -\frac{1}{V}\sum_{N_c} F^{(c)} \otimes L^{(c)}, \tag{2}$$

where $\bar{\sigma}$ is the average stress in the measurement sphere, V is the volume of the measurement sphere, N_c is the number of contacts in the measurement sphere or on the boundary, $F^{(c)}$ is the contact force vector, $L^{(c)}$ is the branch vector joining the centroids of the two particles in contact, and $\otimes$ denotes outer product.

3.1.1. Vertical and Radial Stresses. Figure 4 shows the distribution of vertical stress along the stone column under different settlements. On the whole, the vertical stress increases with the increase of settlement. When the settlement is more than 1000 mm, the stress on the top of stone column decreases significantly. This is because the horizontal constraint of the aggregates on the top of column is small, and the effective volume of the measurement sphere (ID = 14) is decreasing due to the increase of settlement. The vertical stress firstly increases and then decreases along the stone column, which means that the vertical load is transferred from the column to the surrounding soil. At the beginning, the maximum stress is about at the 200 mm below the column top; with the increase of settlement, it gradually moves down to 500 mm. The vertical load on the column is transferred downward, but not to the bottom of the column.

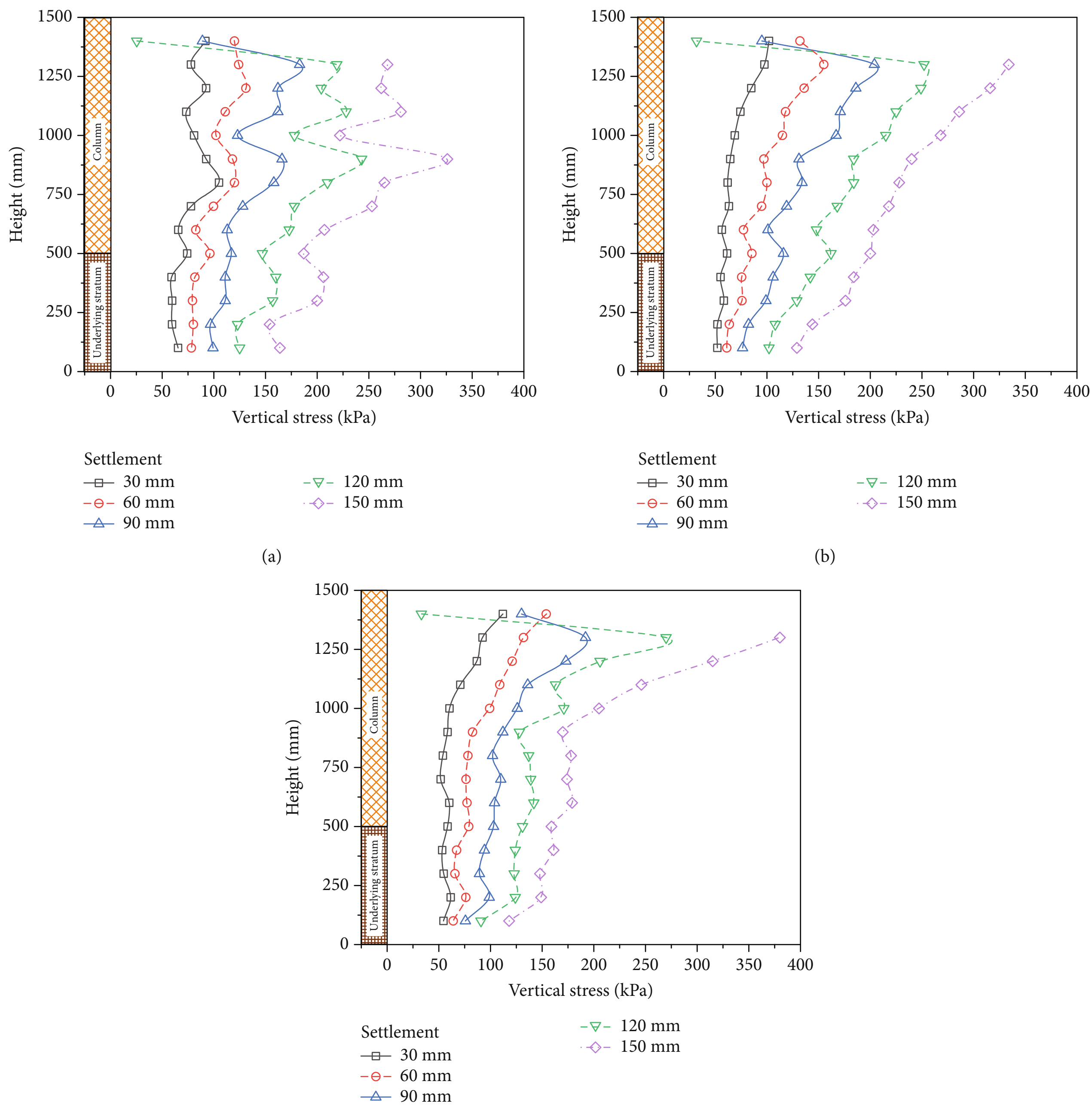

Figure 9: Vertical stresses of the soft soil: (a) 180 mm, (b) 280 mm, and (c) 350 mm away from the center of the column.

Figure 5 shows the distribution of radial stresses along the stone column under different settlements. As shown in the figure, the maximum radial stress occurs within the range of 400 mm below the column top. With the increase of settlement, the radial stress also increases, but the affected area does not increase.

3.1.2. Porosity Change. The change of porosity is an important index of stone column. It can reflect the change of relative density of the column during loading. However, the exact variation of porosity is difficult to obtain in laboratory and field tests. The measurement sphere in PFC can easily measure the change of porosity with time. Porosity is the ratio of the volume of the void in the measurement sphere to the volume of the whole measurement sphere. Four measurement spheres are selected at the model heights of 700 mm, 900 mm, 1100 mm, and 1300 mm. The four positions correspond to 200 mm, 400 mm, 600 mm, and 800 mm in the column, respectively.

Figure 6 shows the porosity changes of the column during loading. The initial porosity of stone column is 0.37, which increases to 0.425 immediately after the initial

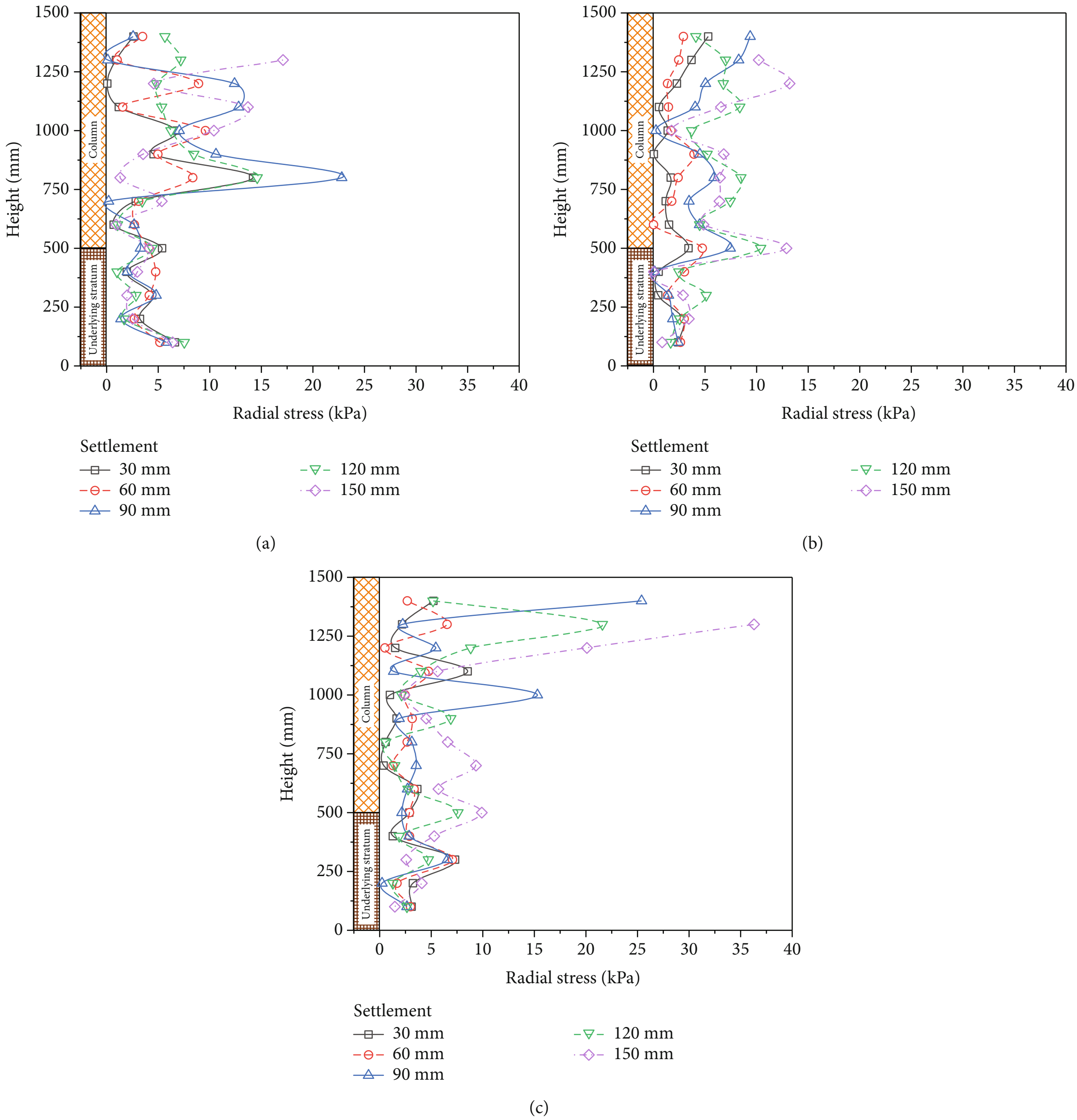

Figure 10: Radial stresses of the soft soil: (a) 180 mm, (b) 280 mm, and (c) 350 mm away from the center of the column.

pressure is applied. As the load continues to increase, the porosity of the three lower positions changes little and is basically stable between 0.41 and 0.42. The porosity of the upper position is stable at about 0.42, when settlement is less than 750 mm. When the settlement is greater than 700, the porosity increases with the increase of settlement. This indicates that when the settlement is less than 750 mm, the aggregates of the column are relatively dense. As the load continues to increase, the lower part of the column remains stable, and the upper part shows sign of failure.

3.1.3. Coordination Number. The coordination number is the average number of active contacts for each particle in a measurement sphere and is computed as

$$C_n = \frac{\sum_{N_b} n_c^{(b)}}{N_b}, \tag{3}$$

where C_n is coordination number, N_b is the number of particles with centroids in the measurement sphere, and $n_c^{(b)}$ is the number of active contacts of particle b.

The coordination number can be used to estimate the particle movement of the column. Four measurement spheres at the model heights of 700 mm, 900 mm, 1100 mm, and 1300 mm are selected. The four positions correspond to 200 mm, 400 mm, 600 mm, and 800 mm in the column, respectively. Figure 7 shows the coordination number in the column during loading. After the initial pressure was applied, the coordination number at the heights of 700 mm, 900 mm, 1100 mm, and 1300 mm was 4.9, 4.7, 4.5, and 4.0. As the load gradually increases, the coordination number of the four positions has some fluctuations, but the coordination number increases in general, which means that the aggregates became denser. At the end of loading, the coordination number at the height of 700 mm, 900 mm, 1100 mm, and 1300 mm was 4.7, 4.6, 4.3, and 3.8. The aggregates at the upper part of the column have a small coordination number, which also mean that the aggregates are relatively loose. This is consistent with the result of porosity.

3.1.4. Deformation. The deformation of the column can reflect the failure mode intuitively. However, it is difficult to monitor the deformation process of stone column under load in laboratory test and in situ engineering practice. Numerical simulation can overcome this disadvantage and conveniently obtain the deformation of column under various loads. PFC 3D obtained the deformation of the column during loading, as shown in Figure 8. Under the action of load, the column is constantly compressed and expanded. Expansion becomes smaller from top to bottom. The deformation of the upper part of the column is large, and the radial stress is also large, which shows a certain positive correlation. When the settlement reaches 1500 mm, the shape of the column is close to the frustum of a cone. The results of the PFC numerical simulation are similar to those of the experiments [20, 21]. Wang et al. [20] and Guo et al. [21] conducted the model test of stone column under uniform load on the entire top of model. The deformation of stone column under rigid foundation is different from that under load only on the column top. When the load only applies on the column top, obvious expansion deformation will occur below the column top [29, 33]. This difference is related to the confined strength of the soil. When the load is applied to both column and soil, the soil can provide greater confined strength than when the load is applied only to the column.

3.2. Vertical and Radial Stresses of the Soft Soil. The vertical and radial stresses of the soft soil during loading are obtained using measurement spheres at different positions. Figure 9 shows the vertical stresses of the soft soil 180 mm, 280 mm, and 350 mm away from the center of the column. Figure 9(a) shows that the vertical stress fluctuates along the depth direction. This is because the soil in this area is close to the column and is greatly affected by the deformation of the column. The vertical stress distributions of the soft soil are relatively regular in Figures 9(b) and 9(c). The vertical stresses in Figure 9 all increase with the increase of load. At the same position away from the center of the column, the vertical stress decreases with the increase of

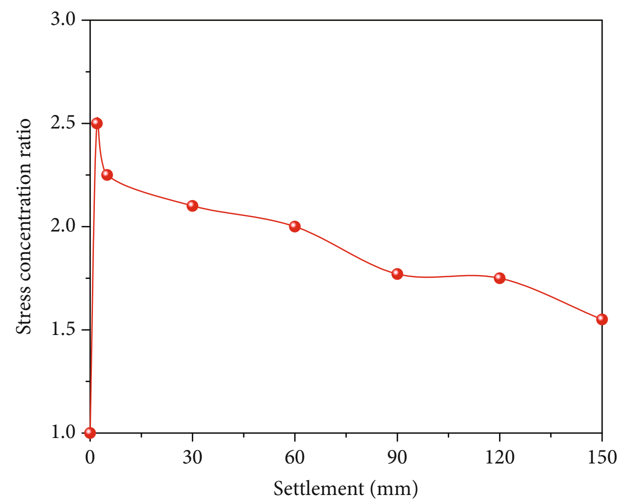

Figure 11: Stress concentration ratio with settlement.

the depth. As the loading plate gradually moves down, the volume of the measurement sphere at the top gradually decreases, so the stress measured by the measurement sphere at the top also decreases.

Figure 10 shows the radial stresses of the soft soil 180 mm, 280 mm, and 350 mm away from the center of the column. Figures 10(a) and 10(c) show that the radial stress of the upper part of the soil is relatively large. Figure 10(b) shows that the radial stress fluctuation of the soil in the middle is large, but the value of radial stress is small. At the height of 500 mm, that is, the position of column foot, the radial stress increases significantly.

The distribution of vertical and radial stress of the soft soil under rigid foundation is different from that load only on the column top. When load is only on the column top, the vertical stress increases along the depth, and the radial stress in the upper soil near the side boundary is large [47].

3.3. Column-Soil Interaction

3.3.1. Stress Concentration Ratio. The stress concentration ratio is an important parameter in geotechnical engineering, which reflects the load sharing between column and soil. In this study, a circular loading plate and an annular loading plate are generated to record the load on the column and soil, respectively. The stress concentration ratio can be obtained by calculating the recorded load. Figure 11 shows that the stress concentration ratio decreases with the increase of settlement. After the initial pressure applied, the stress concentration ratio reaches the maximum of 2.5. This is because the column had higher stiffness than the surrounding soil and carried more load. With the gradual increase of load, the settlement becomes larger, and the stress is transferred from the column to soil. When settlement reached 150 mm, the stress concentration ratio is 1.55. The results in this study are in the range of 2 to 4, which is consistent with other's literature [10, 26]. In Zhang et al.'s article, the typical stress concentration ratio of a stone column-improved ground under rigid foundation is 2 to 4

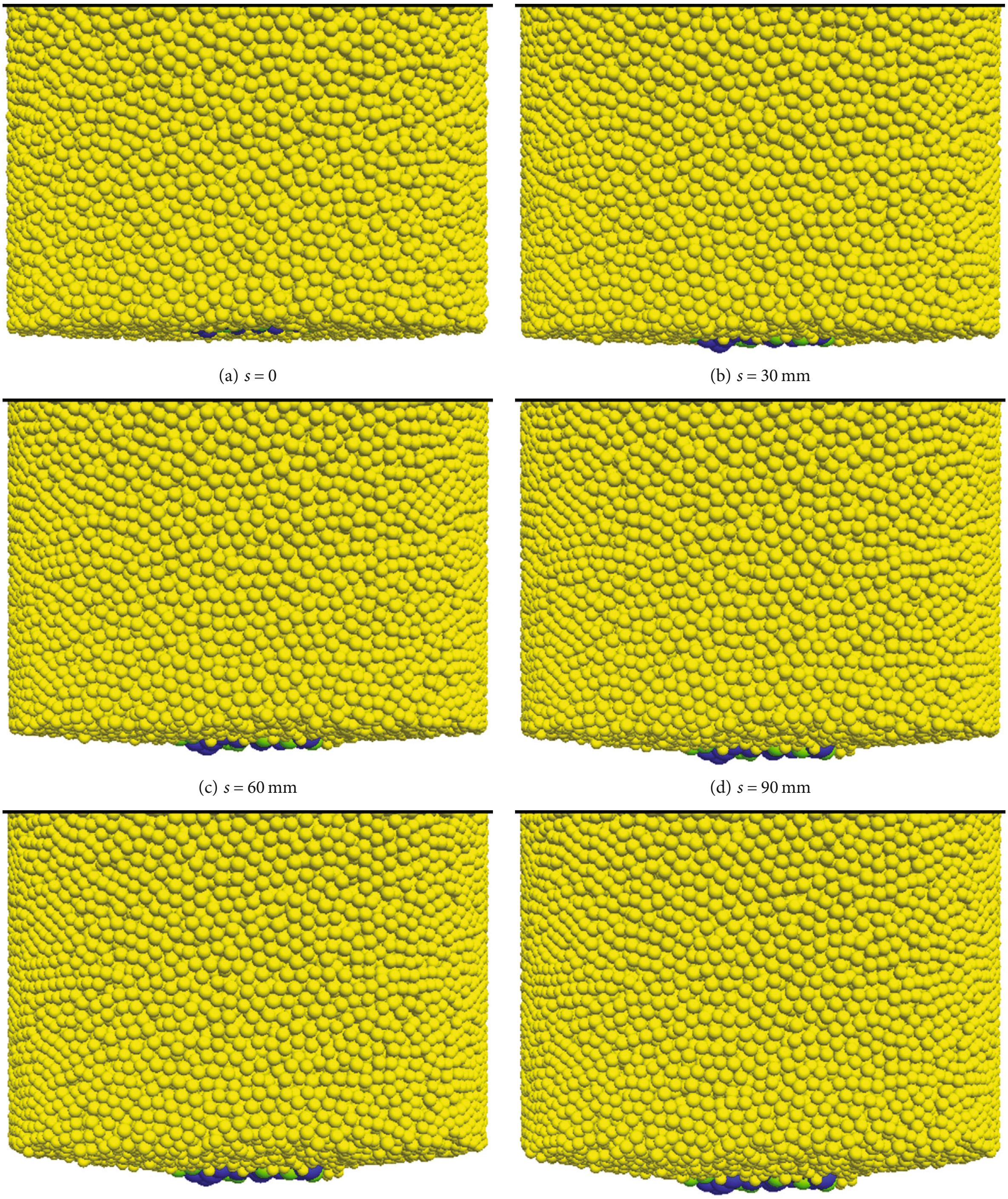

(a) $s = 0$ (b) $s = 30\,\mathrm{mm}$

(c) $s = 60\,\mathrm{mm}$ (d) $s = 90\,\mathrm{mm}$

(e) $s = 120\,\mathrm{mm}$ (f) $s = 150\,\mathrm{mm}$

Figure 12: Deformation of column and soil at the bottom of column during loading.

[26]. When the settlement is greater than 90 mm, the stress concentration ratio is less than 2. This is due to the expansion of the column top; the circular loading plate cannot record accurately. The stress concentration ratio at the later stage of loading is an approximate value.

3.3.2. Deformation of Column and Soil at the Bottom of Column. PFC has the advantage to monitor the movement of particles under load. Each particle can be divided into different groups before loading. Therefore, the trajectory of particles can be clearly seen during loading. In this study, as shown in Figure 2 the particles of soft clay are divided into two groups with different colors. The soil with yellow is the same height as the column. Figure 12 shows the deformation of column and soil at the bottom of column under different settlements. With the increase of load, the deformation of column and soil becomes larger, and the protrusion is more obvious. When the settlement reaches 150 mm, the protrusion is close to cone. The column does not penetrate into the underlying stratum, and the column has a drag effect on the surrounding soil. In other words, the column and surrounding soil deform cooperatively, showing certain integrity. This is related to the large coefficient of friction between column and soil. The stress is transmitted from inside to outside through the column to the surrounding soil, thus making the protrusion to cone shape.

4. Discussion

Although the proposed DEM model can analyze the behavior of a floating stone column under rigid foundation, it still needs to be improved in the following aspects: (1) the linear contact model was used to simulate the soil particle for simplicity; the use of PFC to simulate soft soil requires further study; (2) the displacement-control method was adopted in the model, and the load-control method could be developed in further study; and (3) when the column top expanded during loading, the loading plate on the column did not expand simultaneously.

5. Conclusions

In this present work, a 3D DEM model of a floating stone column under rigid foundation is established. The aggregates of stone column and soft clay are simulated with particles, using the linear contact model. Two loading plates at the same position with the same velocity are used to simulate the rigid foundation. The stress and deformation of column and soft clay are investigated in this study. The interaction between column and soil is also analyzed. Based on the numerical simulation results, the following conclusions have been obtained:

(i) The vertical stress of the column increases with the increase of settlement and decreases with the depth of the column. The radial stress of the column also increases with the settlement, but the affected area is concentrated in the shallow section

(ii) With the settlement increasing, the porosity of the shallow section of the column increases and the coordination number is relatively small. This means that the aggregates in the upper part of the column become loose as settlement increases. The porosity and coordination number of the lower section of the column remain relatively stable with the increase of settlement. Therefore, the aggregates in the lower part remain relatively dense

(iii) Under rigid foundation, the surrounding soil can provide great lateral strength. The expansion deformation of the column decreases gradually from top to bottom

(iv) The vertical stress of the soft clay increases with the increase of settlement. The radial stress of the upper part of soft clay is large, and at the position of column foot, the radial stress increases significantly

(v) The stress concentration ratio decreases from 2.5 to 1.55 during loading. The column does not penetrate into the underlying stratum, and the column drags the surrounding soil down

Data Availability

The data used to support the findings of this study are available from the corresponding author upon request.

Conflicts of Interest

The authors declare that they have no known competing financial interests or personal relationships that could have appeared to influence the work reported in this paper.

Acknowledgments

This research was financially supported by the National Natural Science Foundation of China (grant numbers 51778575 and 52078457).

References

[1] B. A. McCabe, G. J. Nimmons, and D. Egan, "A review of field performance of stone columns in soft soils," *Geotechnical Engineering*, vol. 162, no. 6, pp. 323–334, 2009.

[2] O. Sadaoui and R. Bahar, "Field measurements and back calculations of settlements of structures founded on improved soft soils by stone columns," *European Journal of Environmental and Civil Engineering*, vol. 23, no. 1, pp. 85–111, 2019.

[3] S. Pal and K. Deb, "Effect of stiffness of stone column on drainage capacity during soil liquefaction," *International Journal of Geomechanics*, vol. 18, no. 3, article 04018003, 2018.

[4] A. W. Stuedlein and R. D. Holtz, "Bearing capacity of spread footings on aggregate pier reinforced clay," *Journal of Geotechnical and Geoenvironmental Engineering*, vol. 139, no. 1, pp. 49–58, 2013.

[5] A. W. Stuedlein and R. D. Holtz, "Displacement of spread footings on aggregate pier reinforced clay," *Journal of Geotechnical and Geoenvironmental Engineering*, vol. 140, no. 1, pp. 36–45, 2014.

[6] Y. Wang, Y. F. Yi, C. H. Li, and J. Q. Han, "Anisotropic fracture and energy characteristics of a Tibet marble exposed to multi-level constant-amplitude (MLCA) cyclic loads: a lab-scale testing," *Engineering Fracture Mechanics*, vol. 244, article 107550, 2021.

[7] A. M. Hanna, M. Etezad, and T. Ayadat, "Mode of failure of a group of stone columns in soft soil," *International Journal of Geomechanics*, vol. 13, no. 1, pp. 87–96, 2013.

[8] J. M. O. Hughes, N. J. Withers, and D. A. Greenwood, "A field trial of the reinforcing effect of a stone column in soil," *Geotechnique*, vol. 25, no. 1, pp. 31–44, 1975.

[9] R. A. Barron, "Consolidation of fine-grained soils by drain wells by drain wells," *Transactions of the American Society of Civil Engineers*, vol. 113, no. 1, pp. 718–742, 1948.

[10] J. Han and S. L. Ye, "Simplified method for consolidation rate of stone column reinforced foundations," *Journal of*

Geotechnical and Geoenvironmental Engineering, vol. 127, no. 7, pp. 597–603, 2001.

[11] L. Wang, A. Zhou, Y. F. Xu, and X. H. Xia, "Consolidation of unsaturated composite ground reinforced by permeable columns," *Computers and Geotechnics*, vol. 125, article 103706, p. 14, 2020.

[12] H. B. Poorooshasb and G. G. Meyerhof, "Analysis of behavior of stone columns and lime columns," *Computers and Geotechnics*, vol. 20, no. 1, pp. 47–70, 1997.

[13] J. Han, S. Oztoprak, R. L. Parsons, and J. Huang, "Numerical analysis of foundation columns to support widening of embankments," *Computers and Geotechnics*, vol. 34, no. 6, pp. 435–448, 2007.

[14] Y. Wang, B. Zhang, B. Li, and C. H. Li, "A strain-based fatigue damage model for naturally fractured marble subjected to freeze-thaw and uniaxial cyclic loads," *International Journal of Damage Mechanics*, no. article 105678952110216, 2021.

[15] K. H. Xie, M. M. Lu, and G. B. Liu, "Equal strain consolidation for stone columns reinforced foundation," *International Journal for Numerical and Analytical Methods in Geomechanics*, vol. 33, no. 15, pp. 1721–1735, 2009.

[16] R. Moradi, A. Marto, A. S. A. Rashid, M. M. Moradi, A. A. Ganiyu, and S. Horpibulsuk, "Bearing capacity of soft soil model treated with end-bearing bottom ash columns," *Environmental Earth Sciences*, vol. 77, no. 3, p. 100, 2018.

[17] D. Muir Wood, W. Hu, and D. F. T. Nash, "Group effects in stone column foundations: model tests," *Geotechnique*, vol. 50, no. 6, pp. 689–698, 2000.

[18] A. Cimentada, A. da Costa, J. Cañizal, and C. Sagaseta, "Laboratory study on radial consolidation and deformation in clay reinforced with stone columns," *Canadian Geotechnical Journal*, vol. 48, no. 1, pp. 36–52, 2011.

[19] J. Black, V. Sivakumar, and J. D. McKinley, "Performance of clay samples reinforced with vertical granular columns," *Canadian Geotechnical Journal*, vol. 44, no. 1, pp. 89–95, 2007.

[20] Y. Wang, C. H. Li, and J. Q. Han, "On the effect of stress amplitude on fracture and energy evolution of pre-flawed granite under uniaxial increasing-amplitude fatigue loads," *Engineering Fracture Mechanics*, vol. 240, article 107366, 2020.

[21] P. Guo, F. Liu, G. Lei et al., "Predicting response of constructed tunnel to adjacent excavation with dewatering," *Geofluids*, vol. 2021, Article ID 5548817, 2021.

[22] J. Castro, "An analytical solution for the settlement of stone columns beneath rigid footings," *Acta Geotechnica*, vol. 11, no. 2, pp. 309–324, 2016.

[23] A. K. Das and K. Deb, "Experimental and 3D numerical study on time-dependent behavior of stone column-supported embankments," *International Journal of Geomechanics*, vol. 18, no. 4, article 04018011, p. 16, 2018.

[24] A. Thakur, S. Rawat, and A. K. Gupta, "Experimental and numerical investigation of load carrying capacity of vertically and horizontally reinforced floating stone column group," *Geotechnical and Geological Engineering*, vol. 39, no. 4, pp. 3003–3018, 2021.

[25] P. Guo, X. Gong, and Y. Wang, "Displacement and force analyses of braced structure of deep excavation considering unsymmetrical surcharge effect," *Computers and Geotechnics*, vol. 113, article 103102, 2019.

[26] Z. Zhang, J. Han, and G. B. Ye, "Numerical investigation on factors for deep-seated slope stability of stone column-supported embankments over soft clay," *Engineering Geology*, vol. 168, pp. 104–113, 2014.

[27] B. Indraratna, S. Basack, and C. Rujikiatkamjorn, "Numerical solution of stone column–improved soft soil considering arching, clogging, and smear effects," *Journal of Geotechnical and Geoenvironmental Engineering*, vol. 139, no. 3, pp. 377–394, 2013.

[28] J. Castro and M. Karstunen, "Numerical simulations of stone column installation," *Canadian Geotechnical Journal*, vol. 47, no. 10, pp. 1127–1138, 2010.

[29] X. Tan, L. J. Feng, Z. B. Hu, and M. H. Zhao, "Failure modes and ultimate bearing capacity of the isolated stone column in soft soil," *Bulletin of Engineering Geology and the Environment*, vol. 80, no. 3, pp. 2629–2642, 2021.

[30] P. Guo, X. Gong, Y. Wang, H. Lin, and Y. Zhao, "Minimum cover depth estimation for underwater shield tunnels," *Tunnelling and Underground Space Technology*, vol. 115, article 104027, 2021.

[31] X. Tan, L. J. Feng, Z. B. Hu, and M. H. Zhao, "A DEM-FDM coupled numerical study on the deformation and failure process of the isolated stone column in soft soil," *Bulletin of Engineering Geology and the Environment*, vol. 79, no. 4, pp. 1693–1705, 2020.

[32] B. Indraratna, N. T. Ngo, C. Rujikiatkamjorn, and S. W. Sloan, "Coupled discrete element-finite difference method for analysing the load- deformation behaviour of a single stone column in soft soil," *Computers and Geotechnics*, vol. 63, pp. 267–278, 2015.

[33] X. Tan, M. H. Zhao, Z. B. Hu, and L. J. Feng, "Failure process of a single stone column in soft soil beneath rigid loading: numerical study," *International Journal of Geomechanics*, vol. 20, no. 8, article 04020130, p. 13, 2020.

[34] X. Tan, L. J. Feng, Z. B. Hu, and S. M. Abbas, "The equivalent shear strength properties of the composite soil reinforced by stone columns: an FDM-DEM-coupled numerical evaluation," *Environmental Earth Sciences*, vol. 80, no. 4, article 125, p. 12, 2021.

[35] A. Gholaminejad, A. Mahboubi, and A. Noorzad, "Hybrid continuous-discrete modeling of an ordinary stone column and micromechanical investigations," *Geotechnical and Geological Engineering*, vol. 39, no. 4, pp. 3249–3264, 2021.

[36] J. Cheng, H. Zhang, and Z. Wan, "Numerical simulation of shear behavior and permeability evolution of rock joints with variable roughness and infilling thickness," *Geofluids*, vol. 2018, Article ID 1869458, 11 pages, 2018.

[37] Z. Chen, X. Li, L. Weng, S. Wang, and L. Dong, "Influence of flaw inclination angle on unloading responses of brittle rock in deep underground," *Geofluids*, vol. 2019, Article ID 4657645, 16 pages, 2019.

[38] Y. Wu, Q. Liu, A. H. C. Chan, and H. Liu, "Implementation of a time-domain random-walk method into a discrete element method to simulate nuclide transport in fractured rock masses," *Geofluids*, vol. 2017, Article ID 5940380, 13 pages, 2017.

[39] X. Q. Gu, M. S. Huang, and J. G. Qian, "Discrete element modeling of shear band in granular materials," *Theoretical and Applied Fracture Mechanics*, vol. 72, pp. 37–49, 2014.

[40] Y. Wang, W. K. Feng, H. J. Wang, C. H. Li, and Z. Q. Hou, "Rock bridge fracturing characteristics in granite induced by freeze-thaw and uniaxial deformation revealed by AE monitoring and post-test CT scanning," *Cold Regions Science and Technology*, vol. 177, article 103115, 2020.

[41] Z. Li, Y. H. Wang, C. H. Ma, and C. M. B. Mok, “Experimental characterization and 3D DEM simulation of bond breakages in artificially cemented sands with different bond strengths when subjected to triaxial shearing,” *Acta Geotechnica*, vol. 12, no. 5, pp. 987–1002, 2017.

[42] J. Yu, W. Yao, K. Duan, X. Y. Liu, and Y. L. Zhu, “Experimental study and discrete element method modeling of compression and permeability behaviors of weakly anisotropic sandstones,” *International Journal of Rock Mechanics and Mining Sciences*, vol. 134, article 104437, 2020.

[43] J. M. Li, Y. L. Huang, H. Pu et al., “Influence of block shape on macroscopic deformation response and meso-fabric evolution of crushed gangue under the triaxial compression,” *Powder Technology*, vol. 384, pp. 112–124, 2021.

[44] K. C, S. S, R. J. Pillai, and H. Mudavath, “Influence of erodible layer on granular column collapse using discrete element analysis,” *Geomechanics and Geoengineering*, pp. 1–13, 2021.

[45] X. Q. Gu, Z. P. You, J. G. Qian, and W. Y. Li, “The deformation of granular materials under repeated traffic load by discrete element modelling,” *European Journal of Environmental and Civil Engineering*, vol. 24, no. 8, pp. 1135–1160, 2020.

[46] R. X. Zhang, D. Su, G. P. Lei, and X. S. Chen, “Three-dimensional granular column collapse: impact of column thickness,” *Powder Technology*, vol. 389, pp. 328–338, 2021.

[47] M. X. Gu, J. Cui, J. Yuan, Y. Wu, Y. D. Li, and H. Z. Mo, “The stress and deformation of stone column-improved soft clay by discrete element modelling,” *European Journal of Environmental and Civil Engineering*, pp. 1–17, 2020.

[48] J. Han, *Principles and Practice of Ground Improvement*, John Wiley & Sons, Hoboken, NJ, 2015.

[49] A. A.-C. Guéry, F. Cormery, J. F. Shao, and D. Kondo, “A micromechanical model of elastoplastic and damage behavior of a cohesive geomaterial,” *International Journal of Solids and Structures*, vol. 45, no. 5, pp. 1406–1429, 2008.

[50] Z. Y. Yin, “Micromechanics based analytical model for soils: review and development,” *Chinese Journal of Geotechnical Engineering*, vol. 35, pp. 993–1009, 2013.